

PASTA: Pointwise Assessment of Streamline Tractography Attributes

Derek K. Jones,^{1,2*} Adam R. Travis,^{2,3} Greg Eden,² Carlo Pierpaoli,² and Peter J. Basser²

Diffusion tensor MRI tractography aims to reconstruct noninvasively the 3D trajectories of white matter fasciculi within the brain, providing neuroscientists and clinicians with a potentially useful tool for mapping brain architecture. While this technique is widely used to visualize white matter pathways, the associated uncertainty in fiber orientation and artifacts have, to date, not been visualized in conjunction with the trajectory data. In this work, the bootstrap method was used to determine the distributions of diffusion indices such as trace and anisotropy, together with the uncertainty in fiber orientation. A novel visualization scheme was developed to encode this information at each point along reconstructed trajectories. By integrating these schemes into a graphical user interface, a new tool which we call PASTA (Pointwise Assessment of Streamline Tractography Attributes) was created to facilitate identification of artifacts in tractography that would otherwise go undetected. Magn Reson Med 53:1462–1467, 2005. Published 2005 Wiley-Liss, Inc.†

Key words: DT-MRI; artifacts; distribution; visualization; hyper-streamline

In diffusion tensor MRI (DT-MRI), a set of diffusion-weighted (DW) images is collected and used to form estimates of the self-diffusion tensor in each voxel of the imaged volume (1). From the diffusion tensor, one obtains estimates of mean diffusivity, diffusion anisotropy, and fiber orientation. This information has been used in various attempts to infer connectivity within the brain using a variety of algorithms that are generically referred to as tractography (e.g., 2–6). To date, tractography research has focused predominantly on obtaining images that show the trajectories of individual white matter fasciculi. The reconstructed trajectories are represented either as streamlines (e.g., 2,3) or illuminated streamtubes (e.g., 7,8). However, in such representations, which we term here “trajectory-only” visualizations, there is no indication of either the possible variability of diffusion quantities along the tract or the reliability of the tract reconstruction.

In this work, we describe an integrated approach not only to visualizing the trajectory of white matter fasciculi but also to indicating how diffusion indices, including mean diffusivity and anisotropy indices, vary along the

tract. Furthermore, we show how to visualize uncertainty in fiber orientation at each point along the reconstructed tract and the distribution of diffusion indices at each vertex. This visualization proves to be extremely useful in identifying artifacts in the data that would otherwise go unnoticed in trajectory-only visualizations. As we effectively perform a pointwise assessment of streamline tractography attributes, we refer to this whole approach as PASTA.

METHODS

Acquisition

Diffusion-weighted magnetic resonance imaging data were acquired from healthy volunteers on a 1.5-T GE Signa LX system (General Electric, Milwaukee, WI, USA) with 40 mT/m gradients. The acquisition was gated to the cardiac cycle using a peripheral gating device placed on the subjects' forefinger. A multislice peripherally gated EPI acquisition sequence was used, providing nearly isotropic resolution ($1.7 \times 1.7 \times 1.7$ mm) and coverage of the whole head. Eighty-four contiguous axial slice locations with isotropic resolution were acquired using the dual-gradient scheme (9,10). The basic acquisition using this scheme consists of 1 image with no gradients applied and then 6 images in which gradients are applied along the vector directions [+1, +1, 0], [+1, -1, 0], [+1, 0, +1], [+1, 0, -1], [0, +1, +1], [0, +1, -1]. This acquisition sequence was repeated 16 times, resulting in 112 images per slice location. We refer to the data set consisting of all 112 DW images per slice location as the “super-set.” Following motion/distortion correction (11), the diffusion tensor was computed in each voxel and diagonalized to compute the eigenvectors and eigenvalues. The fractional anisotropy (12) was then computed in each voxel and, together with the principal eigenvector, used to create a color-encoded fiber orientation map (13).

Tractography

To perform tractography, as well as to be able to obtain repeated estimates of the tensor field at subvoxel locations, a continuous representation of the diffusion tensor field was established using the *B*-spline approach described by Pajevic et al. (14). This approach provides an extremely rapid method for obtaining subvoxel estimates of the diffusion tensor field. Using the color-encoded maps, voxels lying within a fasciculus of interest were identified and fiber tracking was initiated from these “seedpoints” using a tractography algorithm akin to that of Basser et al. (4) with a step size of 0.5 mm. Tracking was terminated when the fractional anisotropy (FA) fell below 0.20. Note that, since we ultimately aimed to visualize uncertainty in fiber orientation, in contrast with the approach of Basser et al.

¹Centre for Neuroimaging Sciences, Institute of Psychiatry, London, United Kingdom.

²Section on Tissue Biophysics and Biomimetics, Laboratory of Integrative Medicine and Biophysics, National Institute of Child Health and Human Development, National Institutes of Health, Bethesda, Maryland, USA.

³Department of Biomedical Engineering, Vanderbilt University School of Engineering, Nashville, Tennessee, USA.

Grant sponsor: Wellcome Trust; Grant sponsor: Whitaker Foundation.

*Correspondence to: Derek K. Jones, Centre for Neuroimaging Sciences, Institute of Psychiatry, P089, De Crespigny Park, London SE5 8AF, United Kingdom. E-mail: d.jones@iop.kcl.ac.uk

Received 15 September 2004; revised 15 December 2004; accepted 29 December 2004.

DOI 10.1002/mrm.20484

Published online in Wiley InterScience (www.interscience.wiley.com).

(4), the tensor field was not smoothed. As these trajectories were reconstructed from the superset volume, we refer to them as the superset trajectories.

Deriving Vertex-Specific Indices

The various data that were encoded onto the tracts can be classified into two groups: (i) scalar invariant diffusion indices and (ii) uncertainty measures.

Scalar Invariant Diffusion Indices

At each vertex of the reconstructed superset trajectory (i.e., at each 0.5-mm step), the diffusion tensor was estimated and several scalar indices were computed including trace, FA (12), and the indices of tensor linearity, planarity, and sphericity developed by Westin et al. (15).

Uncertainty Measures

To derive uncertainty measures, we used the bootstrap method in a manner similar to that described elsewhere (16). The superset acquisition consisted of 16 repetitions of each of the 7 images acquired with the dual-gradient scheme. From these 112 images, subset volumes were created by sampling (with replacement) 6 images from each of the 7 bins, creating a DT-MRI volume with 42 images per slice. One thousand such volumes were created in this way. By establishing a continuous representation of the tensor field for each bootstrapped volume (14), the principal eigenvector at each vertex of the superset trajectory was computed. From the 1000 estimates of the principal eigenvector thus obtained, the 95% cone of uncertainty was computed according to the dyadic approach described previously (16).

Trajectory Visualization

The superset trajectories were visualized in MATLAB using illuminated tubes as described elsewhere (8). Finally, we initiated tracking from the seedpoint for each bootstrapped volume, thereby obtaining 1000 trajectory estimates from a particular seedpoint. These were represented both as streamlines and as translucent streamtubes such that the density of bootstrapped trajectories passing through a region was reflected by the opacity of the resultant visualization.

Visualizing Parameters along the Trajectories

The vertex-specific measures were encoded onto the trajectories in two ways. In the first method, the trajectories were represented using polygonal cylinders whose long axes were coincident with the tangent to the reconstructed trajectory with appropriate lighting added to enhance the 3D visualization. At each vertex, the facets of the polygonal cylinder were colored according to the index of interest. In the second method, an approach closely related to the hyperstreamline approach of Delmarcelle and Hesselink (17) was used. In this approach, the major axis of the hyperstreamline is coincident with the principal eigenvector, while the width of the tube varies in proportion to the second and third eigenvalues. Similarly, in our approach, the width of the tube varies in proportion to the diffusion indices of interest, such as the 95% cone of uncertainty.

Testing Distributions for Normality

It has been shown previously that the eigenvalues of the diffusion tensor (and consequently the trace, since it is a linear sum of the three eigenvalues) have a Gaussian distribution if the only source of perturbation in the diffusion-weighted images used to estimate the diffusion tensor is Gaussian random noise (23). Consequently, any deviation from normality indicates an additional source of perturbation in the data. We therefore compared the distributions of the three eigenvalues and of the trace of the tensor (obtained from the 1000 bootstrap estimates) at each vertex using the Kolmogorov–Smirnov test (KS test). Essentially, the KS test takes each value of the experimental distribution (in our case, 1000 bootstrapped samples) and compares the proportion less than this with the number expected if the data had come from the standard normal distribution. We refer to the maximal difference between the experimental and the normal distribution as the KS statistic. The KS test was performed using the function `kstest` in MATLAB (The Mathworks, Natick, MA, USA) with an α value of 0.05.

Graphical User Interface

To facilitate ease of visualization, a graphical user interface (GUI) was developed to allow rapid toggling between measures of interest, as well as toggling between colored streamtubes and hyperstreamline visualizations. Furthermore, the GUI allowed simultaneous plotting of the various measures of interest as a function of arc length along the trajectory.

RESULTS AND DISCUSSION

The key features of the PASTA GUI are presented in Fig. 1, in which a streamtube representing a reconstructed trajectory passing through the body of the corpus callosum has been encoded for fractional anisotropy. Note the heterogeneity of the index along the trajectory. Color coding the anisotropy along tracts has been previously reported elsewhere (7). The streamtubes color-encoded for trace were found to be extremely informative. Since the trace has been shown to be fairly uniform throughout the parenchyma (10), streamtubes color-encoded for trace should have a uniform color as long as they remain within the parenchyma. However, in regions where the tracts pass close to CSF-filled spaces, the trace becomes elevated, suggesting partial volume contamination with CSF. An example is presented in Fig. 2, which shows fibers launched in the body of the corpus callosum and internal capsule. As the fibers of the corpus callosum pass close to the lateral ventricles, their color changes, indicating partial volume contamination. These regions are readily identifiable as “hot spots” on the color-encoded streamtube (Fig. 2f) and also by the large peaks in the profile (Fig. 2b).

Figure 2e shows the same trajectory encoded for the 95% cone of uncertainty in fiber orientation using a hyperstreamline representation, while Fig. 2g shows the bootstrapped trajectories. To a certain extent, the “flare” of the bootstrapped trajectories is seen to be dependent on the cone of uncertainty at each point (although the effect of architectural milieu on bootstrapped trajectories discussed

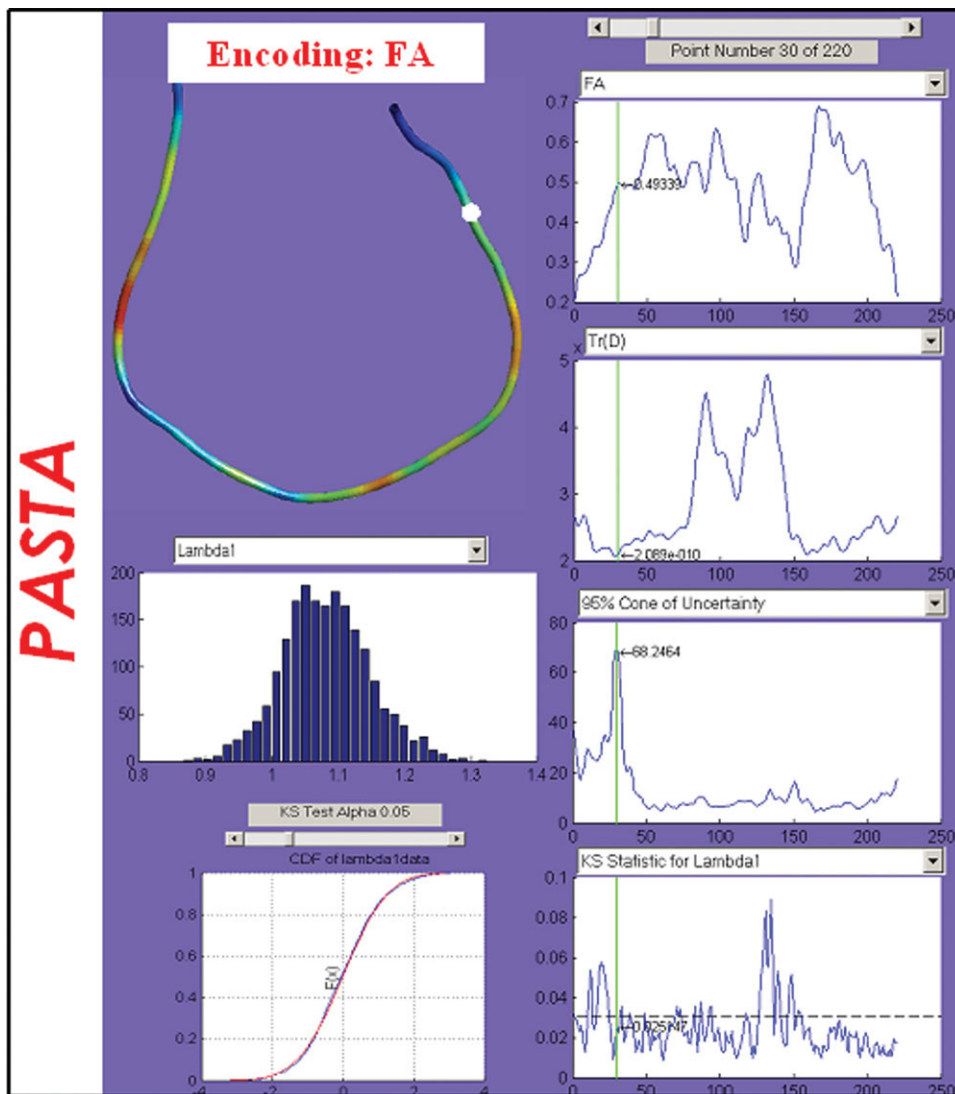


FIG. 1. Key features of the graphical user interface for pointwise assessment of streamline tractography attributes (PASTA).

elsewhere (19) is also an important determinant of the reproducibility of bootstrapped trajectories).

Several lessons can be learned from the profiles in Fig. 2. First, we can see that a large amount of CSF contamination (i.e., the two large peaks identified by the asterisks) does not necessarily mean that the uncertainty in fiber orientation will be greatly elevated. Certainly, it has been shown that suppressing CSF contamination (through the use of the FLAIR technique, for example) can lead to an increase in the measured anisotropy (20) and it has previously been shown that the cone of uncertainty is dependent on anisotropy (16). However, Fig. 2b and c together indicate that regions with large CSF contamination do not necessarily have larger uncertainty in fiber orientation than neighboring “uncontaminated” regions. What can be seen, however, is that a much more important determinant of the uncertainty in fiber orientation is the relationship between the linearity and planarity of the diffusion tensor, as measured using Westin’s indices (15). There is a large spike in the profile of the cone of uncertainty (indicated by α) and this is coincident with the maximal value of C_p (the measure of planarity). In fact, it appears that the cone of un-

certainty increases whenever C_p is comparable with, or exceeds, C_L (the measure of linearity). Another example is the second local maxima indicated by β . This relationship between planarity and the cone of uncertainty is rather intuitive given that, for an oblate tensor (i.e., when the tensor has negatively skewed eigenvalues), the principal diffusion direction is poorly defined. However, we note that many groups (including ourselves) have published tracking results obtained with termination criteria that are based solely on the fractional anisotropy (and sometimes on the angle turned between successive propagation steps). Typically, the tracking is terminated when the fractional anisotropy falls below a certain threshold (e.g., 0.2). The rationale for this is that at values of FA below this threshold, the estimates of fiber orientation become unreliable. Conversely, this inherently implies that in regions where FA is high, estimates of fiber orientation are reliable. Note, however, that the FA in a region of high cone of uncertainty (α in Fig. 2a) is not particularly low (FA = 0.493). This result should therefore serve as a warning to any groups that utilize a simple FA threshold for termination of tracking and indicates the limitation of indices

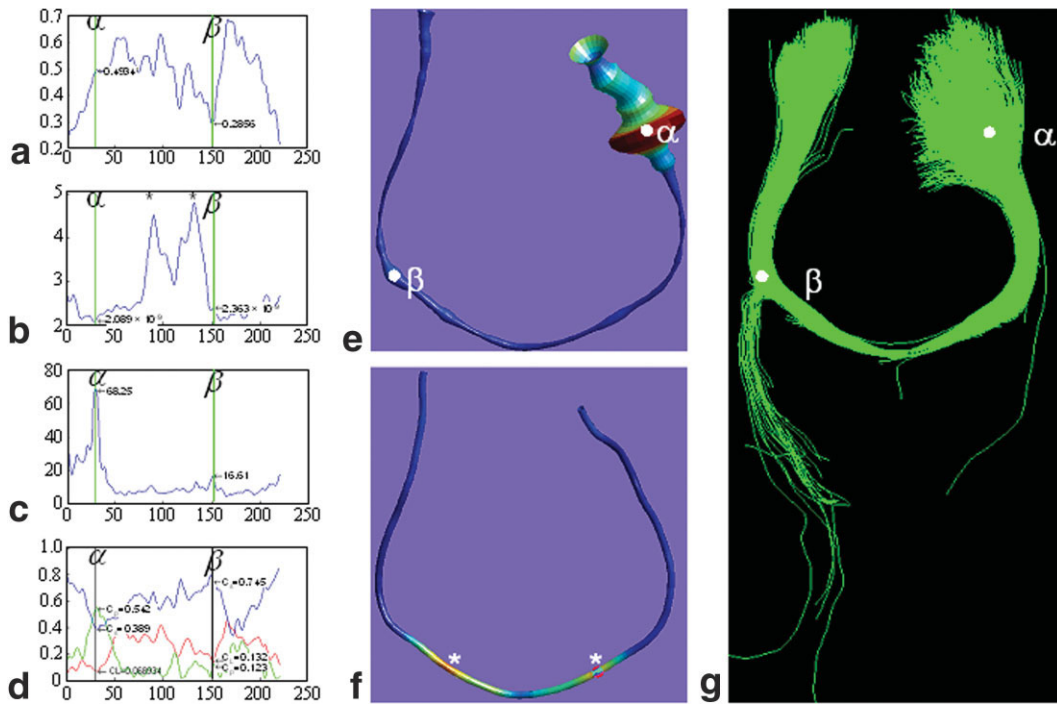


FIG. 2. Demonstration of pointwise assessment of streamline tractography attributes for a seedpoint placed in the body of the corpus callosum. Profiles are shown for the following: (a) Fractional anisotropy; (b) trace (in units of $10^{-9}\text{mm}^2 \text{ s}^{-1}$); (c) 95% cone of uncertainty (in degrees); (d) Westin's measures of sphericity (C_s), planarity (C_p), and linearity (C_l). Note that the profiles display the arc length from left to right, but that the fibers are displayed with the point moving from right to left. In (e), the streamline trajectory is represented as a hyperstreamline, where both the color and the width of the hyperstreamline encode the 95% cone of uncertainty. The vertices indicated by α and β correspond to the points on the profile indicated by the same labels in (a–d). In (f), the streamline trajectory is represented as a simple streamtube, with each vertex encoded by the trace. The asterisks indicate the “hot-spots” (regions of high trace) that are also highlighted in (b). (g) shows the streamline trajectories obtained on each bootstrap iteration.

such as FA that do not reflect the skewness or higher moments of the eigenvalues.

Figure 3a shows an additional trajectory encoded for the 95% cone of uncertainty using the hyperstreamline approach, while Fig. 3b shows the superset trajectory together with the bootstrapped trajectories. Note again that the dispersion of the bootstrapped tracts in Fig. 3b is related to the width of the hyperstreamlines in Fig. 3a. At γ in Fig. 3a, the hyperstreamline flares out, which is reflected by a large number of bootstrapped tracts projecting away from the superset trajectory. At δ , the hyperstream-

line flares to a lesser extent and, likewise, fewer bootstrapped tracts deviate from the superset trajectory than at β . The hyperstreamline visualization in Fig. 3a clearly provides a more succinct and readily interpreted visualization than Fig. 3b.

Figure 4 shows the 95% cone of uncertainty hyperstreamlines for a number of tracts launched in the corpus callosum. Note that only the compact portion of the corpus callosum has low uncertainty. As the tracts reach the cortex, the streamtubes “trumpet” out, indicating lower reproducibility in fiber orientation.

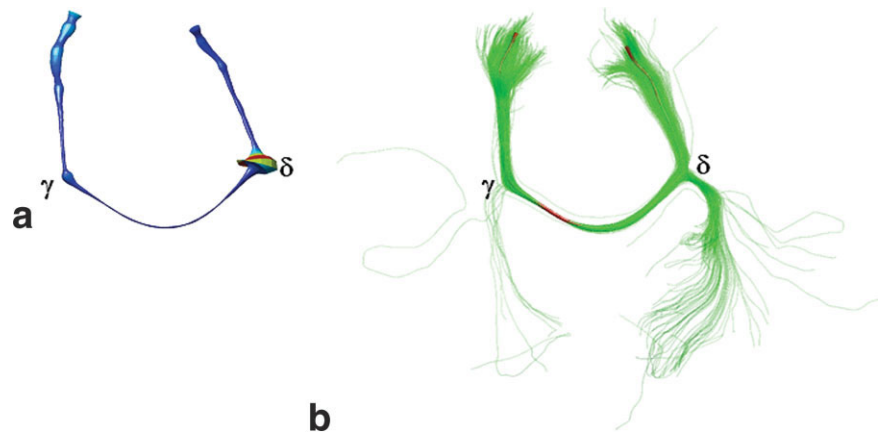


FIG. 3. (a) Hyperstreamline representation of the 95% cone of uncertainty, together with (b) bootstrapped trajectories. Note that at γ , the 95% cone of uncertainty is substantially smaller than at δ . The corresponding points are indicated on the bootstrapped trajectories in (b). The red streamtube that passes through the center of the bootstrap trajectories is the trajectory computed from the superset.

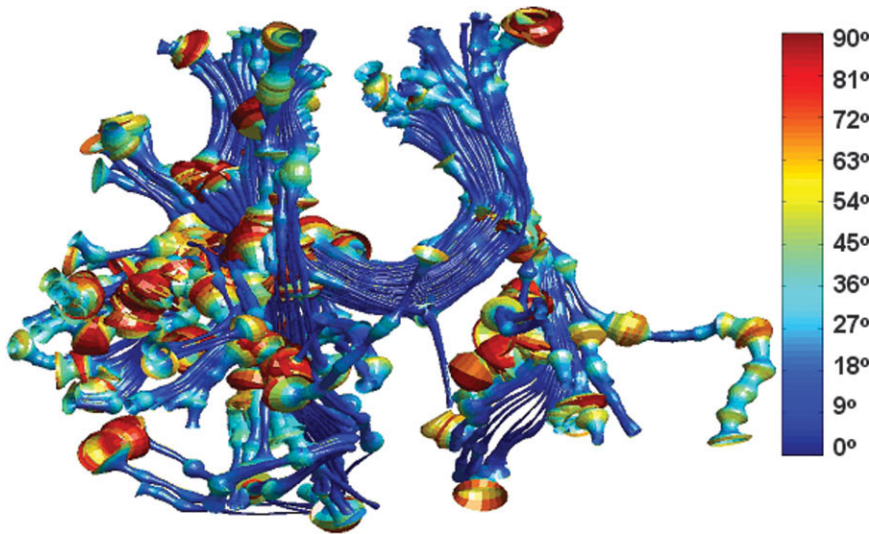
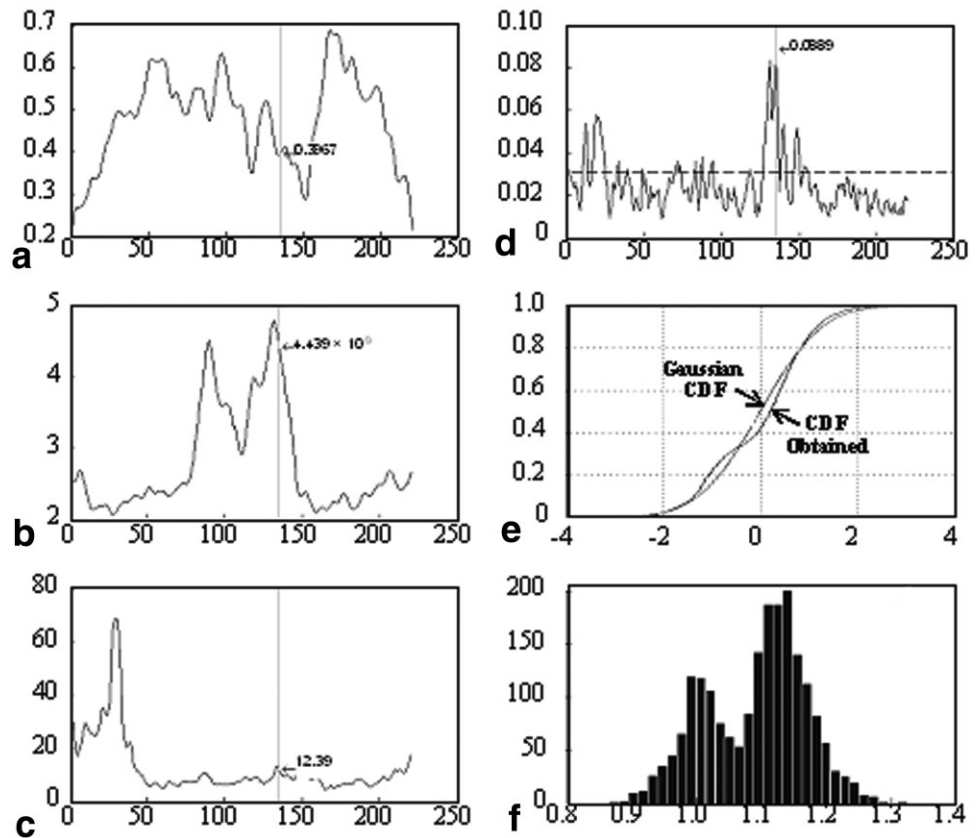


FIG. 4. Hyperstreamline representation of the 95% cone of uncertainty for multiple tracts passing through the corpus callosum. Note the low uncertainty in the body of the corpus callosum and the “trumpeting” of the hyperstreamlines as they approach the cortex.

Figure 5 shows how examining the distribution of diffusion indices can help to indicate potential artifacts. The trajectory shown in this figure is the same as in Figs. 1 and 2. In this example, the profile of the Kolmogorov–Smirnov statistic (Fig. 5a), obtained from testing the distribution of the principal eigenvalue for normality, was used to identify those regions with non-Gaussian behavior (i.e., those where the KS statistic exceeded the critical value represented by the horizontal dashed line) (Fig. 5d). The figure shows the global maximum and in this region, we observe

that the distribution of the largest eigenvalue is bimodal (Fig. 5e). Given that we only fit a single diffusion tensor to the data set, and expect a unimodal Gaussian for trace (18), this result suggests that the spatial location of the vertex has been populated by different tissue types during the acquisition of the bootstrap data. Looking carefully at the nearby location of the spikes in the trace profile (Fig. 5b), it is not hard to imagine the source of the bimodal distribution. The most likely event is that there is some residual motion occurring during the collection of the

FIG. 5. Illustration of the use of PASTA to examine distributions of bootstrapped values at each vertex of a reconstructed streamline. (a) Profile of fractional anisotropy. (b) Profile of trace. (c) Profile of 95% cone of uncertainty. (d) Profile of the test statistic obtained with the Kolmogorov–Smirnov (KS) test for normality of the distribution of the principal eigenvalue. The horizontal dashed line indicates the critical value for the KS, for a two-tailed test with an α value of 0.05. (e) Graphical comparison of the cumulative density function (CDF) for the Gaussian distribution that best fits the data with the empiric distribution of the primary eigenvalue. (f) Histogram of the bootstrapped estimates of the principal eigenvalue at the streamline vertex. A clear bimodal distribution is observed. The vertical line in (a–d) corresponds to the vertex where the largest KS statistic is observed.



bootstrap data set that has not been completely corrected by our motion correction algorithm (11). Examination of distributions in this way therefore serves as a sensitive way of checking data for residual motion. Note that there is only a minor “ripple” in the cone of uncertainty profile at this location (Fig. 5c), which indicates that the uncorrected motion cannot necessarily be identified from the cone of uncertainty data alone.

We note that an alternative method to the bootstrap method for estimating the orientational uncertainty in fiber orientation has recently been proposed (21). With well-behaved data (i.e., in which the only source of perturbation is Johnson RF noise), this approach can be shown to provide estimates of uncertainty that are comparable with those obtained from the bootstrap. However, the approach used in the current work, by definition, incorporates all sources of perturbations in the estimates of uncertainty and, more importantly, confers the additional advantages of being able to examine the distributions of parameters for deviations from idealized behavior (see Fig. 5) and to identify CSF partial volume artifacts.

Finally, as we have previously suggested (16), the bootstrap could be used to compare the efficiency of different tensor smoothing and regularization techniques (e.g., 14,22,23), which aim to eliminate (noise-induced) variations in estimates of fiber orientation while preserving true anatomic variations. In the current framework, the hyperstreamline visualization approach would allow one to visualize the efficiency of these approaches more readily as both anatomic and uncertainty information is viewed concurrently. As such, our PASTA and Poupon’s “spaghetti plate” (22) form a nice complement!

CONCLUSION

In this work we have developed a novel visualization approach that enhances the interpretability of DT-MRI tractography reconstructions. This approach enables, for the first time, the visualization of relevant diffusion characteristics (i.e., trace, Westin indices) along specific white matter trajectories within the brain. This visualization is useful as it provides a much more informative anatomic context than that offered by 2D planar representations. This is especially true for tracts that follow a tortuous 3D trajectory. In addition to these general diffusion characteristics, the associated cone of uncertainty in fiber orientation can also be visualized, allowing the user to determine how much confidence to assign to the tract reconstruction at each point.

Fiber tracking using DT-MRI has recently received wide attention in the medical community, as it can potentially provide (noninvasively) maps of the “wiring” of the brain and therefore has promise in many fields including psychiatry and neurology. However, because tractography representations have been limited primarily to trajectory-only visualizations, there is a real danger of mistaking artifact for architecture. The approach reported in the current work aims to ameliorate this problem by providing clinicians and scientists with a much more informed position from which to view and interpret tract reconstructions from DT-MRI.

ACKNOWLEDGMENTS

We thank Liz Salak for editing the manuscript.

REFERENCES

1. Basser PJ, Mattiello J, Le Bihan D. MR diffusion tensor spectroscopy and imaging. *Biophys J* 1994;66:259–267.
2. Mori S, Crain BJ, Chacko VP, van Zijl PC. Three dimensional tracking of axonal projections in the brain by magnetic resonance imaging. *Ann Neurol* 1999;45:265–269.
3. Conturo TE, Lori NF, Cull TS, Akbudak E, Snyder AZ, Shimony JS, McKinstry RC, Burton M, Raichle ME. Tracking neuronal fiber pathways in the living human brain. *Proc Natl Acad Sci USA* 1999;96:10422–10427.
4. Basser PJ, Pajevic S, Pierpaoli C, Duda J, Aldroubi A. In vivo tractography using DT-MRI data. *Magn Reson Med* 2000;44:625–632.
5. Parker GJM. Tracing fiber tracts using fast marching. In: Proceedings of the 8th Annual Meeting of ISMRM, Denver, 2000. p. 85.
6. Behrens TEJ, Johansen-Berg H, Woolrich MW, Smith SM, Wheeler-Kingshott CAM, Boulby PA, Barker GJ, Sillery EL, Sheehan K, Ciccarelli O, Thompson AJ, Brady JM, Matthews PM. Non-invasive mapping of connections between human thalamus and cortex using diffusion imaging. *Nat Neurosci* 2003;6:750–757.
7. Zhang S, Curry C, Morris DS, Laidlaw DH. Visualizing diffusion tensor MR images using streamtubes and streamsurfaces. In: Proceedings of the IEEE Visualization Conference, Utah, 2000.
8. Catani M, Howard R, Pajevic S, Jones DK. Virtual in vivo interactive dissection of white matter fasciculi in the human brain. *NeuroImage* 2002;17:77–94.
9. Davis TL, Wedeen VJ, Weisskoff, Rosen BR. White matter tract visualization by echo-planar MRI. In: Proceedings of the 12th Annual Meeting of SMRM, New York, 1993. p. 289.
10. Pierpaoli C, Jezzard P, Basser PJ, Barnett A, Di Chiro G. Diffusion tensor MR imaging of the human brain. *Radiology* 1996;201:637–648.
11. Rohde GK, Barnett AS, Basser PJ, Marengo S, Pierpaoli C. Comprehensive approach for correction of motion and distortion in diffusion-weighted MRI. *Magn Reson Med* 2004;51:103–114.
12. Basser PJ, Pierpaoli C. Microstructural and physiological features of tissue elucidated by quantitative-diffusion-tensor MRI. *J Magn Reson B* 1996;111:209–219.
13. Pajevic S, Pierpaoli C. Color schemes to represent the orientation of anisotropic tissues from diffusion tensor data: application to white matter fiber tract mapping in the human brain. *Magn Reson Med* 1999;43:526–540. (Erratum appears in *Magn Reson Med* 1999;43:921).
14. Pajevic S, Aldroubi A, Basser PJ. A continuous tensor field approximation of discrete DT-MRI data for extracting microstructural and architectural features of tissue. *J Magn Reson* 2002;154:85–100.
15. Westin CF, Peled S, Gudbjartsson H, Kikinis R, Jolesz FA. Geometrical diffusion measures for MRI from tensor basis analysis. In: Proceedings of the 5th Annual Meeting of ISMRM, Vancouver, Canada, 1997. p 1742.
16. Jones DK. Determining and visualizing uncertainty in estimates of fiber orientation from diffusion tensor MRI. *Magn Reson Med* 2003;49:7–12.
17. Delmarcelle T, Hesselink L. Visualizing second-order tensor fields with hyperstreamlines. *IEEE Comput Graph Appl* 1993;13:25–33.
18. Pajevic S, Basser PJ. Parametric and non-parametric statistical analysis of DT-MRI data. *J Magn Reson* 2003;161:1–14.
19. Jones DK, Pierpaoli C. Towards a marriage of deterministic and probabilistic tractography methods: bootstrap analysis of fiber trajectories in the human brain. In: Proceedings of the 12th Annual Meeting of ISMRM, Kyoto, Japan, 2004. p 1276.
20. Papadakis NG, Martin KM, Mustafa MH, Wilkinson ID, Griffiths PD, Huang CL-H, Woodruff PWR. Study of the effect of CSF suppression on white matter diffusion anisotropy mapping of healthy human brain. *Magn Reson Med* 2002;48:394–398.
21. Behrens TE, Woolrich MW, Jenkinson M, Johansen-Berg H, Nunes R, Clare S, Matthews PM, Brady JM, Smith SM. Characterization and propagation of uncertainty in diffusion weighted MR imaging. *Magn Reson Med* 2003;50:1077–1088.
22. Poupon C, Clark CA, Frouin V, Regis J, Bloch I, Le Bihan D, Mangin J. Regularization of diffusion-based direction maps for the tracking of brain white matter fasciculi. *NeuroImage* 2000;12:184–195.
23. Coulon O, Alexander D, Arridge SR. Principal diffusion direction field regularisation for diffusion tensor magnetic resonance images. In: Proceedings of the 9th Annual Meeting of ISMRM, Glasgow, Scotland, 2001. p 125.